Electronic Supplementary Information (ESI)

Degradable Copper(II)-Doped Starch-Based Biopolymeric Films with Antibacterial Activity

Kiryl I. Trusau,[a,b] Paula Jorge,[c,d] Ana Catarina Sousa,[a,e] Tiago A. Fernandes,[a] Vânia André,[a] Marina V. Kirillova,[a] Andrew I. Usevich,[b] Nuno Cerca, *[c,d] and Alexander M. Kirillov*[a]

[a.] *Centro de Química Estrutural, Institute of Molecular Sciences, Departamento de Engenharia Química, Instituto Superior Técnico, Universidade de Lisboa, Av. Rovisco Pais, 1049-001 Lisboa, Portugal; kirillov@tecnico.ulisboa.pt*
[b.] *Department of Oil and Gas Processing and Petroleum Chemistry, Belarusian State Technological University, 13a Sverdlova St., 220006 Minsk, Belarus*
[c.] *Centre of Biological Engineering, University of Minho, Campus de Gualtar, 4710-057 Braga, Portugal; nunocerca@ceb.uminho.pt*
[d.] *LABBELS–Associate Laboratory, Braga/Guimarães, Portugal*
[e.] *Área Departamental de Engenharia Química, ISEL-Instituto Superior de Engenharia de Lisboa, Instituto Politécnico de Lisboa, 1959-007 Lisboa, Portugal*

Electronic Supplementary Information (ESI) contains: Materials and methods, antibacterial assays, microscope images of crystalline samples (Figure S1) and crystal data (Table S1) of **1**–**3**; TGA data (Figure S2); PXRD patterns (Figure S3); coupons of $[PS]_n$ and $[PS\text{-}MCC]_n$ biopolymeric films (Figure S4); ATR-FTIR spectra and discussion (Figures S5–S13), SEM-EDS data and discussion (Figures S14–S16); water absorption data (Table S2); Cu release tests (Table S3); additional antibacterial activity data (Figures S17–S19, Table S4). Crystallographic data in CIF format (CCDC 2177365-2177367).

Materials and Methods. All chemicals and solvents were purchased from commercial sources. FTIR-ATR spectra were recorded on a Shimadzu IRAffinity-1S apparatus equipped with an ATR ZnSe Performance Crystal Plate accessory. Absorbance spectra were collected in the 4000–650 cm^{-1} range with a 2.0 cm^{-1} resolution using 64 co-added scans (abbreviations: vs − very strong, s − strong, m – medium, w – weak, br – broad, sh − shoulder). Particle size of **1**–**3** was determined by wet dispersion (water) on a Mastersizer 3000 (Malvern Panalytical). EA (elemental analyses) were run on a Perkin Elmer PE 2400 Series II analyzer by Laboratory of Analyses of IST. SEM and SEM-EDX was acquired using a Thermo Scientific, Phenom ProX G6 Desktop SEM, with the accelerating voltage of 25.0 kV. For copper release studies, the determination of Cu content was performed by ICP-OES (Perkin Elmer Optical Emission Spectrometer Optima 2000 DV) with the following operation conditions: RF power 1300 W, auxiliary gas flow 0.2 $L{\cdot}min^{-1}$, nebulizer gas flow 0.6 $L{\cdot}min^{-1}$, plasma flow 15 $L{\cdot}min^{-1}$, Sample Flow Rate 1.50 $mL{\cdot}min^{-1}$, and Cu analytical line 327.393 nm (LAIST, Laboratory of Analyses, IST). Thermogravimetric analysis (TGA) experiment was carried out on Metler Toledo TGA/DSC-1/1600 HF in the temperature range between 30 and 500 °C and at a heating rate 3 °C/min under oxygen atmosphere.

Antibacterial Assays. The antimicrobial activity of compounds **1**, **2**, and **3** and their doped films were evaluated using a soft agar overlay assay. Bacteria were grown in MHB II overnight and then inoculated into warm soft MHA II (0.5% agar) at the final concentration of $1{\times}10^6$ colony forming units (CFU) mL^{-1}. In a 9 cm Petri dish, 3 mL of this inoculum were placed on top of 10 mL of solidified hard MHA II (1.7% agar). An average of 4 mg of each compound and their respective doped films (cut to round discs with 0.9 cm of diameter) were placed on top of the soft MHA II and incubated for 24h. Films without Cu-dopant and those with CuO were used as controls. Antibacterial activity was observed when a halo of no bacterial growth around the samples was present. In order to quantitatively compare samples, inhibition halos were analysed by photographing the plates in a Bio-Rad ChemiDoc™ Imager and measuring the minimum inhibition radius in the image editing software GIMP. Measurements were analysed and plotted using Excel and GraphPad softwares. Data was normalized for the molar content of copper(II) in each sample. The non-normalized results are given in Figures S17−S19.

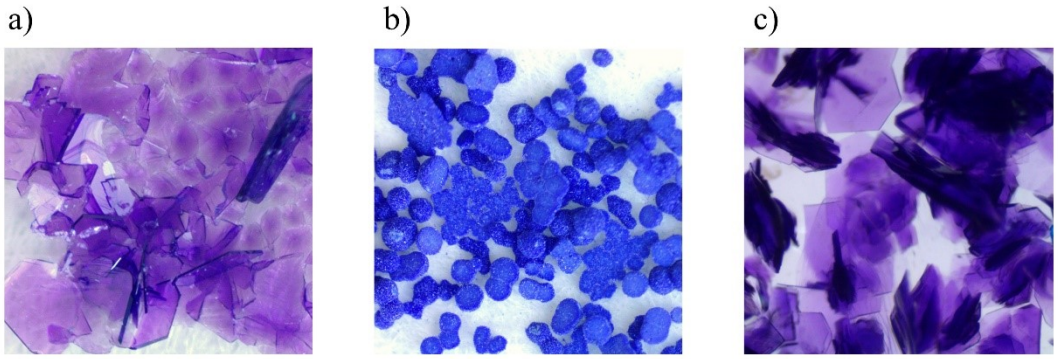

Figure S1. Microscope images of the crystalline samples of **1** (a), **2** (b), and **3** (c) taken using an Olympus stereomicroscope system SZ61.

Table S1. Crystal Data and Structure Refinement Details for **1**–**3**.

	1	**2**	**3**
formula	$C_{22}H_{20}CuN_2O_4$	$C_{12}H_{12}CuN_2O_4$	$C_{14}H_{14}CuN_2O_5$
fw	943.8(4)	311.78	353.82
Crystal form, color	Plate, purple	Plate, blue	Plate, purple
Crystal size (mm)	0.4 × 0.2 × 0.01	0.3 × 0.15 × 0.05	0.18 × 0.10 × 0.04
Crystal system	Monoclinic	Triclinic	Monoclinic
Space group	$P2_1/c$	$P1$	$C2/c$
a, Å	18.005(4)	4.1453(3)	27.018(7)
b, Å	5.9694(13)	6.0280(5)	5.7985(13)
c, Å	8.7828(18)	11.9507(9)	8.912(2)
α, deg	90	95.652(4)	90
β, deg	91.219(8)	93.881(4)	91.287(14)
γ, deg	90	98.430(4)	90
Z	2	1	4
V, Å^3	943.8(4)	292.94(4)	1395.8(6)
T, K	293	293	293
D_c, g cm^{-3}	1.548	1.767	1.684
μ(Mo Kα), mm^{-1}	1.190	1.876	1.591
θ range (°)	2.263 – 32.081	3.437 – 28.297	3.017 – 32.026
refl. collected	30492	8936	7304
independent refl.	2634	1451	2361
R_{int}	0.1006	0.0773	0.0438
R_1 [a], wR_2 [b] [$I \geq 2\sigma(I)$]	0.0657, 0.0871	0.0434, 0.0709	0.0383, 0.0859
GOF on F^2	1.139	1.076	1.025

[a] $R_1 = \Sigma||F_o| - |F_c||/\Sigma|F_o|$. [b] $wR_2 = [\Sigma[w(F_o^2 - F_c^2)^2]/\Sigma[w(F_o^2)^2]]^{1/2}$

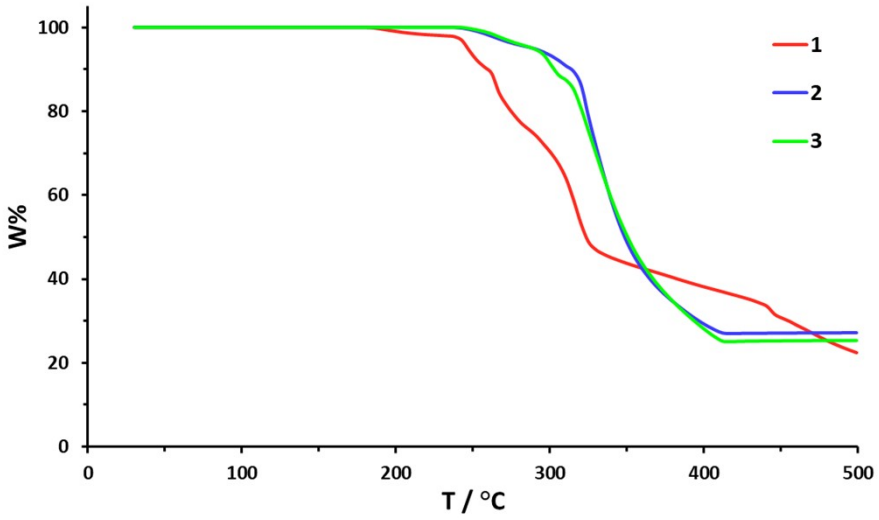

Figure S2. TGA curves of **1**–**3**.

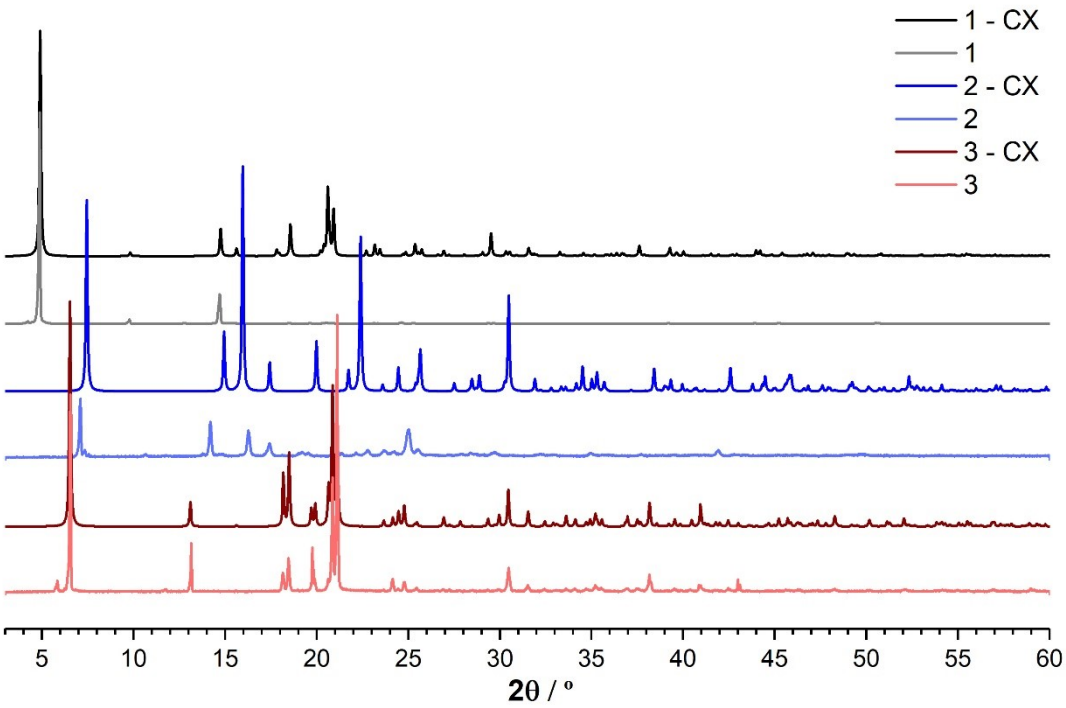

Figure S3. Experimental (light-colored) and theoretical (dark-colored, CX) powder diffraction patterns for **1** (black), **2** (blue) and **3** (red).

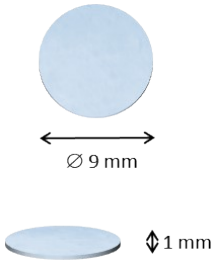

Figure S4. Schematic representation of coupons of $[PS]_n$ or $[PS\text{-}MCC]_n$ biopolymeric films.

FTIR Spectra. The ATR-FTIR spectra of $[PS]_n$ reveal the interaction of potato starch with glycerol plasticizer (Figure S7, SI), as evidenced by a shift of the OH bands. Given a low amount of Cu-dopant, there is no significant variation in the spectra of doped and undoped films (Figures S4−S12), with all the $[PS]_n$-based samples showing characteristic bands at 3300 cm^{-1} $\nu(OH/H_2O)$, 2936 cm^{-1} $\nu(CH)$, and 1647 cm^{-1} $\delta(H_2O)$.[S1,S2] Low intensity bands between 1460 and 1340 cm^{-1} correspond to $\delta(CH_2)$ and $\delta(CH)$, both of which are assigned as modes involving the deformation of the CH_2 group.[S1-S3] Vibrations of the glucosidic C–O–C bond and the complete glucose ring are related with a band at 1151 cm^{-1}. Also, many modes of stretching and bending vibrations, such as $\nu(C–O)$, $\nu(C–O–H)$, or $\delta(C–H)$ can be invoked.[S1] The band at 925 cm^{-1} can be ascribed to the skeletal modes of the C–C stretch, the pyranose ring, and the skeletal mode of the $\alpha(1\rightarrow4)$ glycosidic linkage.[S3]

a)

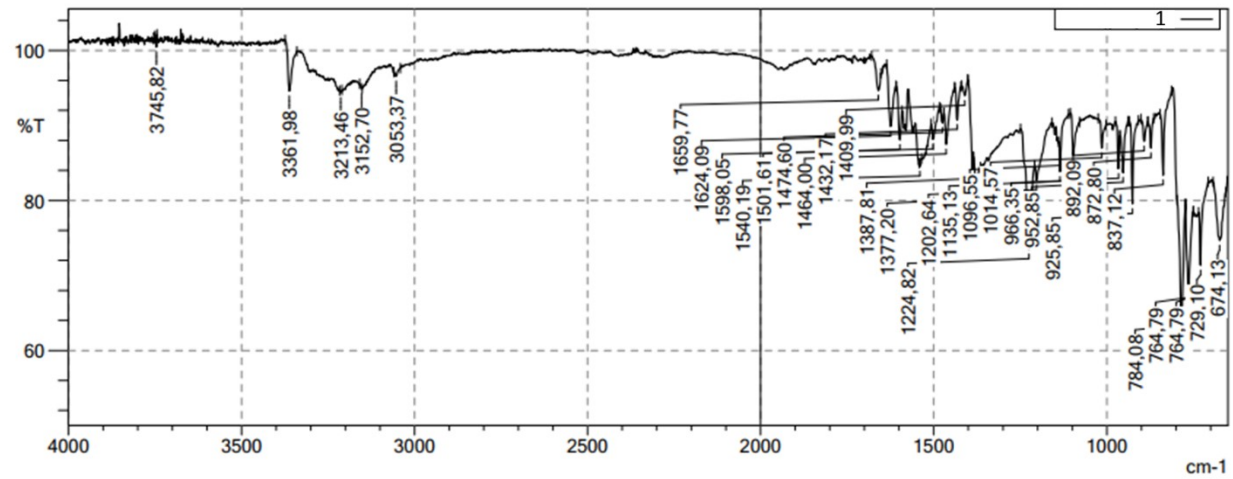

b)

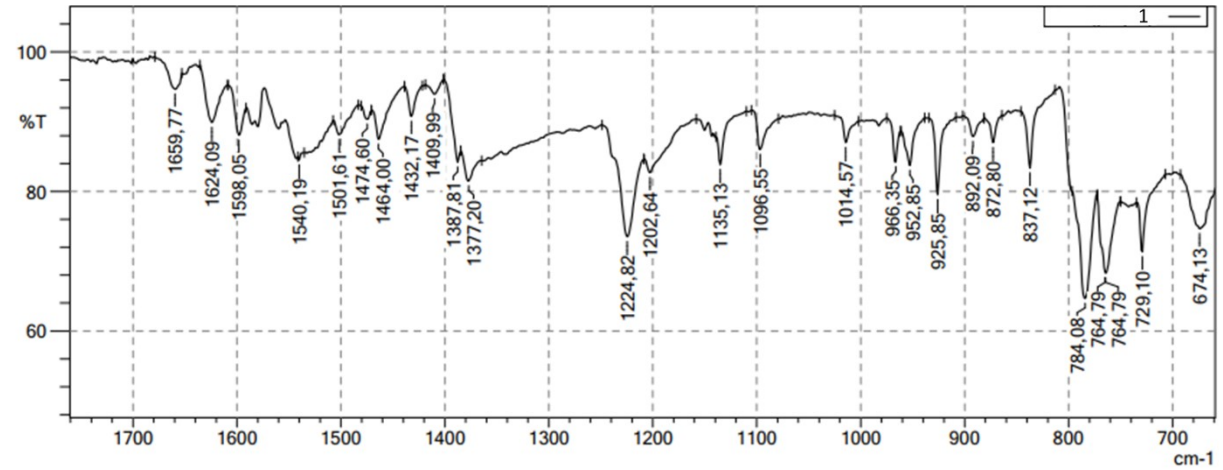

Figure S5. (a) Full FTIR spectrum of **1** and (b) its zoomed fragment (650−1750 cm^{-1}).

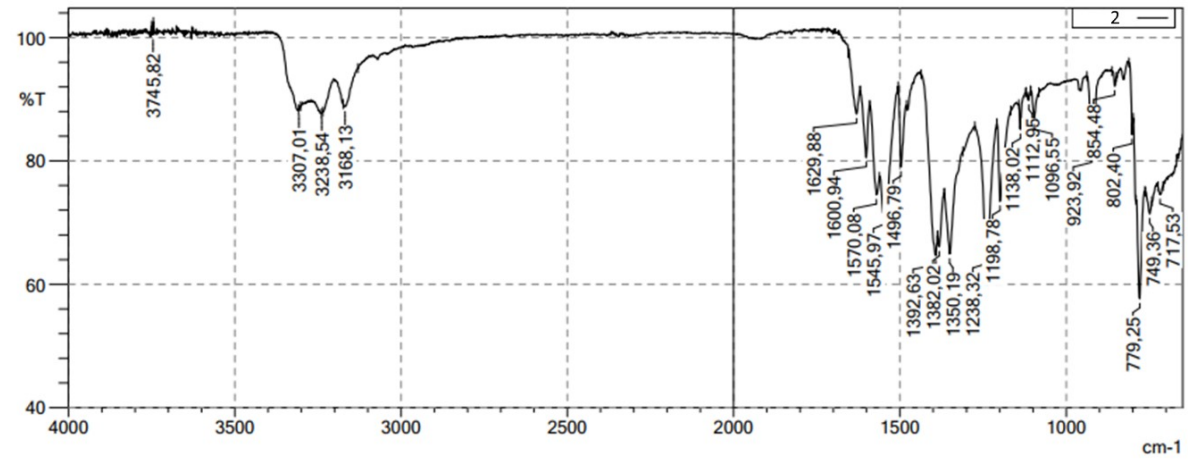

Figure S6. FTIR spectrum of **2**.

a)

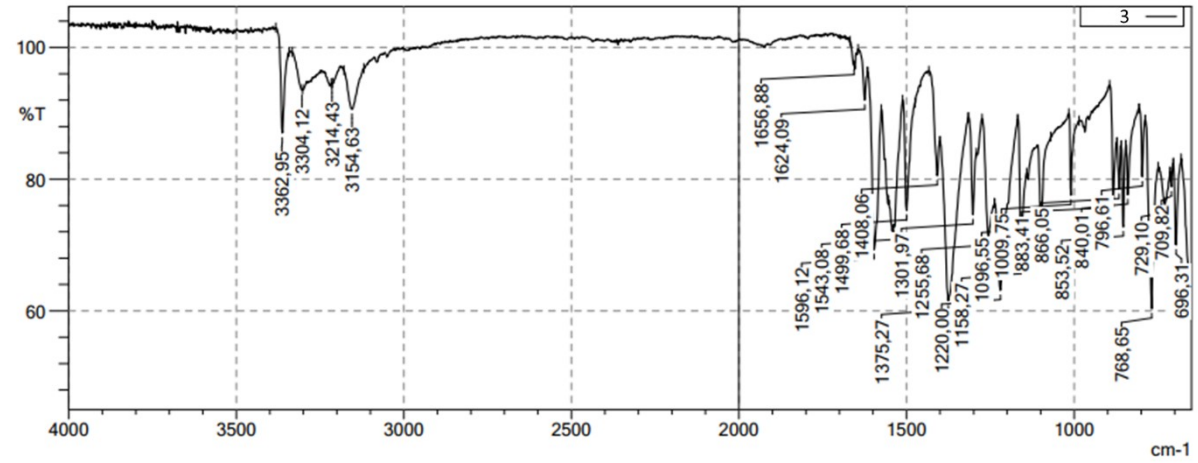

b)

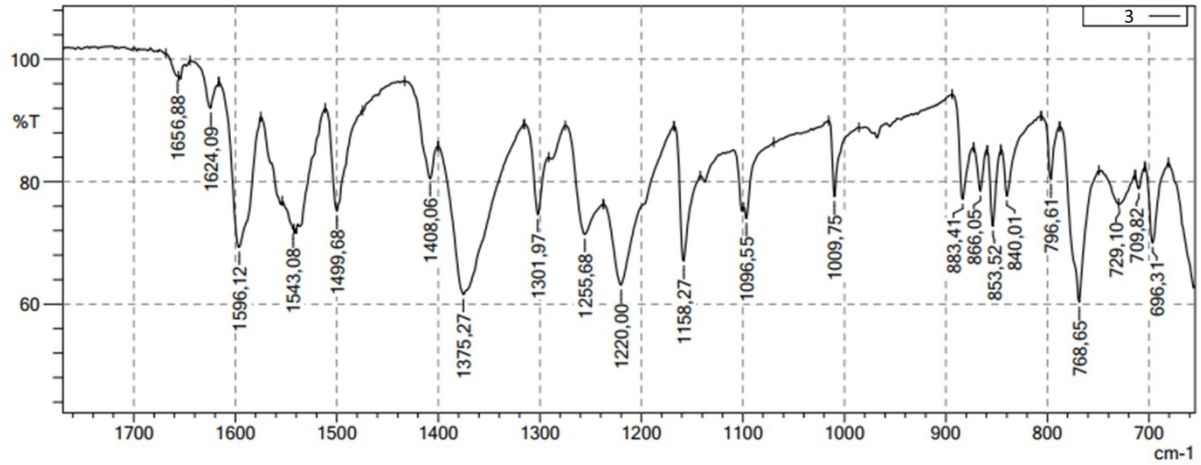

Figure S7. (a) Full FTIR spectrum of **3** and (b) its zoomed fragment (650−1750 cm^{-1}).

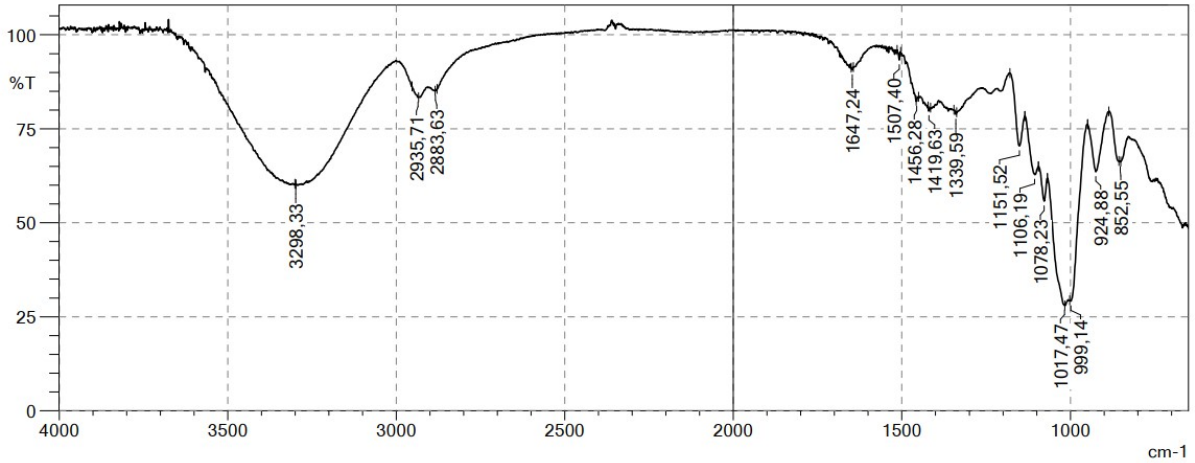

Figure S8. FTIR spectrum of $[PS]_n$.

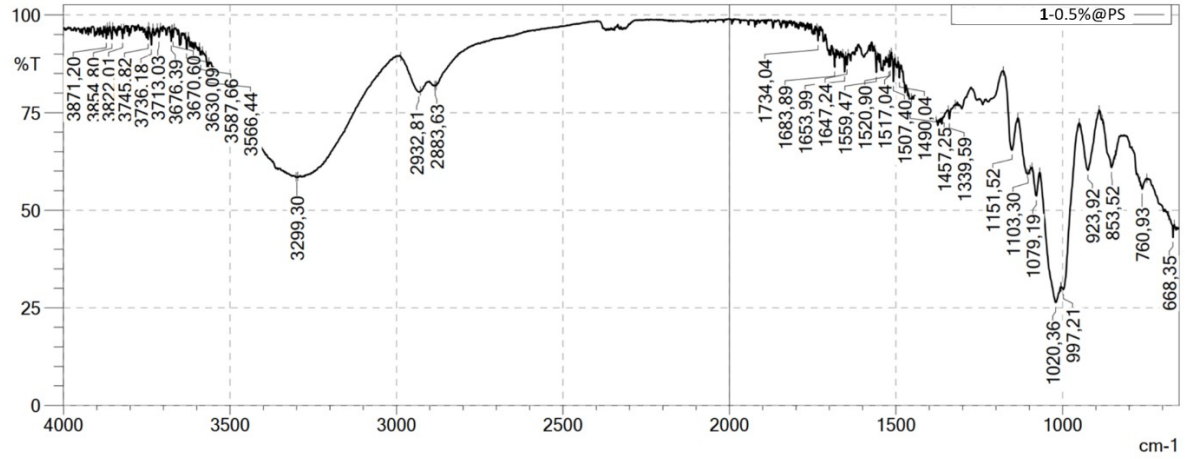

Figure S9. FTIR spectrum of **1**@$[PS]_n$.

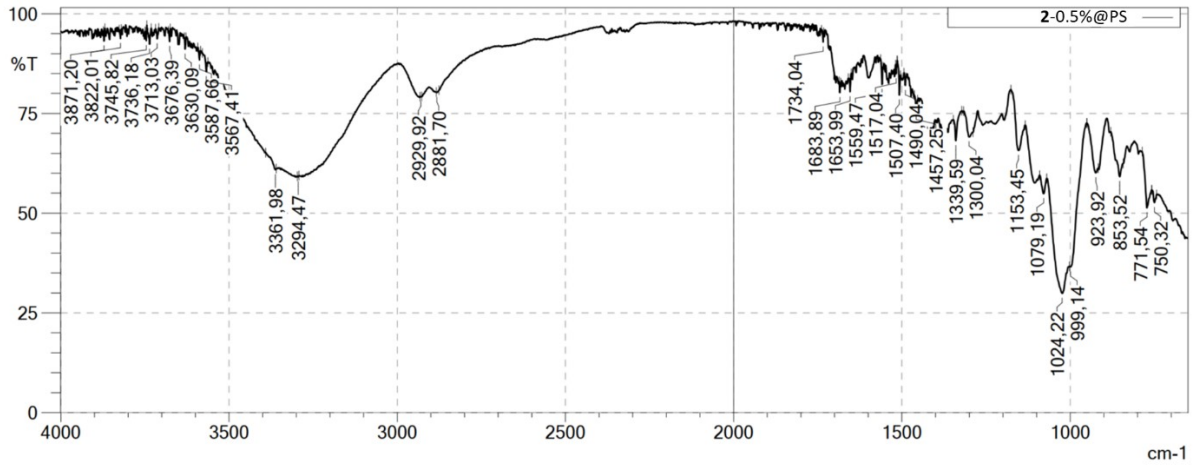

Figure S10. FTIR spectrum of **2**@$[PS]_n$.

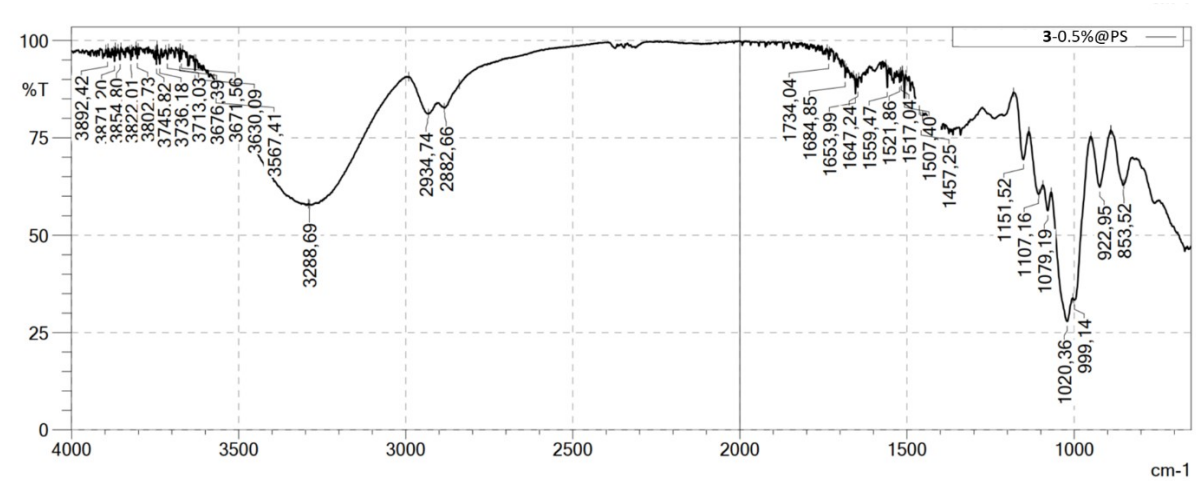

Figure S11. FTIR spectrum of **3**@$[PS]_n$.

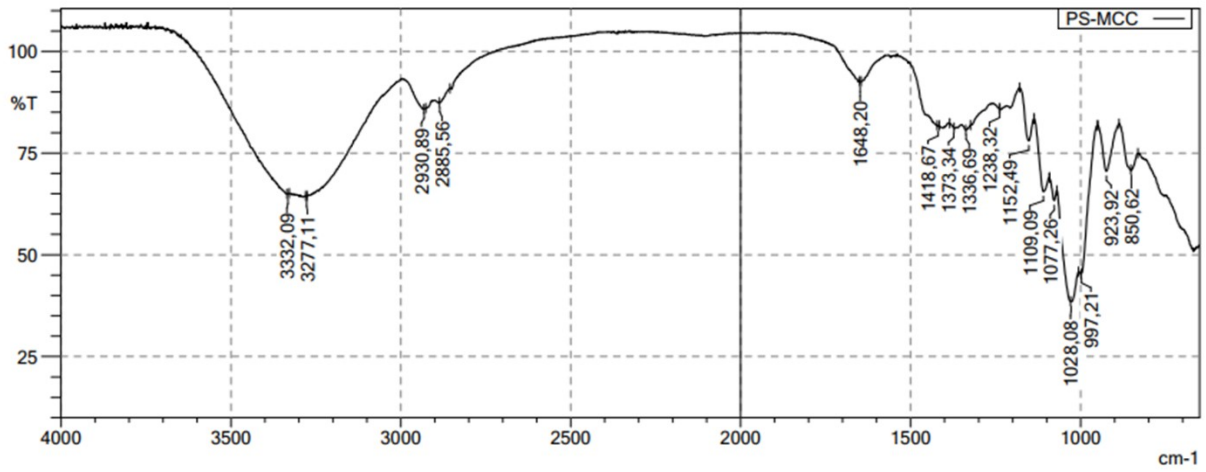

Figure S12. FTIR spectrum of $[PS\text{-}MCC]_n$.

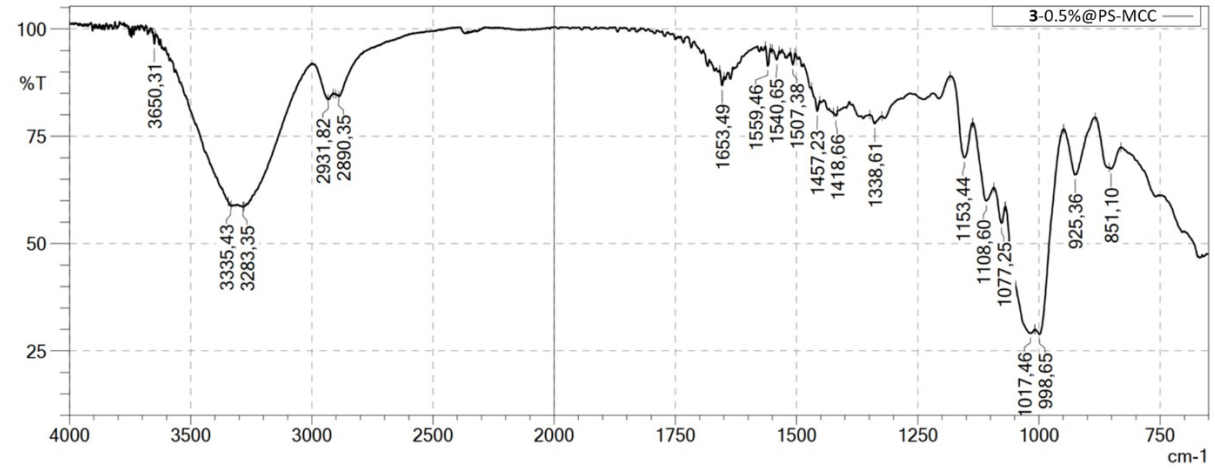

Figure S13. FTIR spectrum of **1**@$[PS\text{-}MCC]_n$.

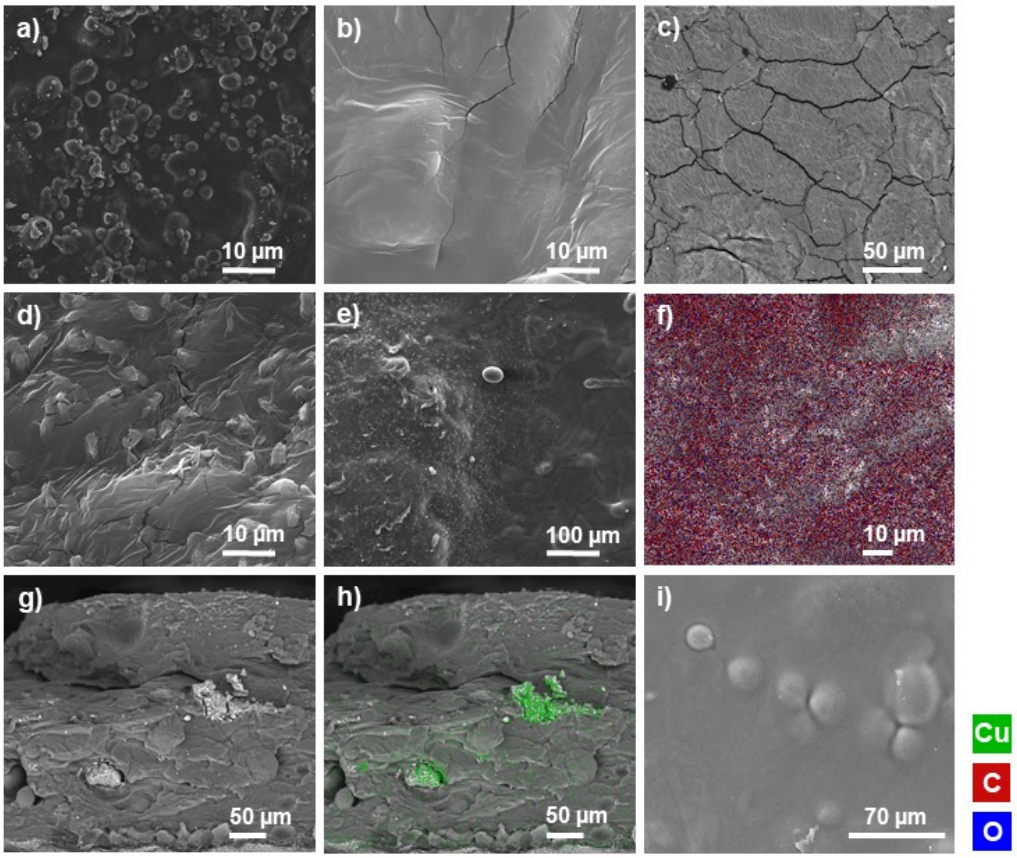

Figure S14. Morphology characterization using SEM-EDX. SEM images: (a) **1**@$[PS]_n$, (b) **1**@$[PS\text{-}MCC]_n$, (c) **2**@$[PS]_n$, (d) **3**@$[PS]_n$, (e) zoom-out of **3**@$[PS]_n$, (f) **3**@$[PS]_n$ with an EDX analysis of Cu, C and O distribution, (g) **2**@$[PS]_n$ cross-section top-down, (h) the same as the region of (g) but with an EDX analysis of Cu distribution (**2**@[PS]); (i) $[PS]_n$ film. Magnification scale: (a), (d), (c), (d), and (h): 1000×; (f) and (i): 500×; (e): 100×.

Morphological Characterization of Cu-doped Biopolymeric Films. SEM–EDX was used to investigate the Cu-doped $[PS]_n$ and $[PS\text{-}MCC]_n$ biopolymeric films (Figure S14, SI). Figures S14a and S14b show the surface of the two different matrices, doped with compound **1**. The inclusion of microcrystalline cellulose resulted in an particularly sludgy surface devoid of the inhomogeneous granules that characterize the $[PS]_n$ surface (Figure 3i). As seen in Figures S14a, S14c, and S14e, different dopants produce very diverse morphologies on the surface of the films. The materials were also studied by SEM–EDX with the copper probe to visualize the distribution of Cu (Figures S14f and S14h). The SEM image of **1**@$[PS]_n$ (Figure S14e) shows that copper is not on the coupon's surface, as was found for other doped films and on both sides. For **2**@$[PS]_n$ (Figures S14g and S14h), the coupon was cut to analyze the cross-section. Figures S14g and S14h present the fragment of **2**@$[PS]_n$ with the particles of coordination

polymer present on the cross-section of the film. Inside the 1 mm thick film, copper is sporadically accumulated in zones comprising bigger particles of **2**. The same effect is observed in other doped films (Figures S15 and S16, SI). Nevertheless, when considering the entire sample coupons used in antibacterial tests, any potential change in the distribution of Cu dopants **1**–**3** is negligible, as evidenced by well reproducible antibacterial tests run in triplicate.

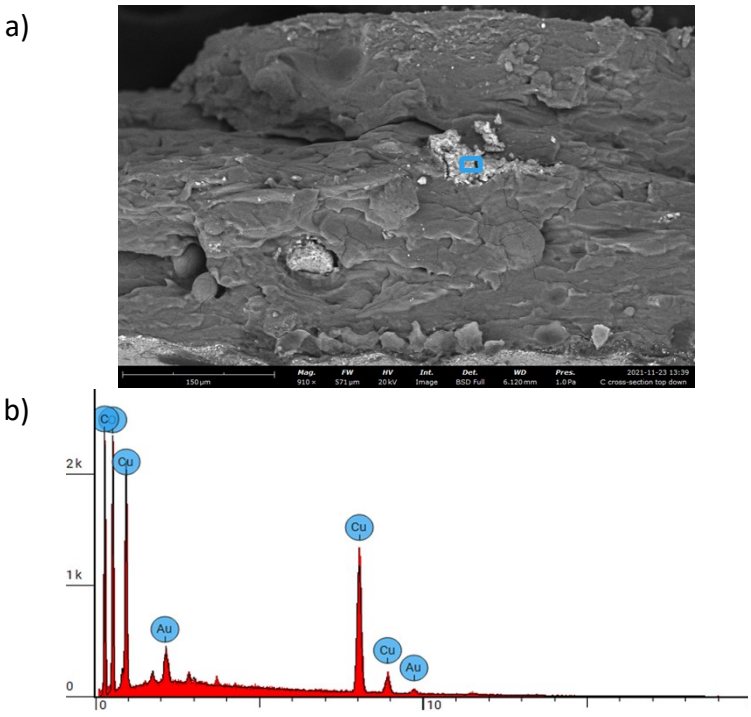

Figure S15. (a) Example of SEM image at 910× magnification of **2**-5%@$[PS]_n$ biopolymeric film with (b) EDS analysis of elemental composition (151 737 counts in 0:00:30 (5 035 c/s)). Blue square in (a) shows an area rich in Cu compound **2** (used for running EDS). The presence of Au in (b) is due to gold SEM coating.

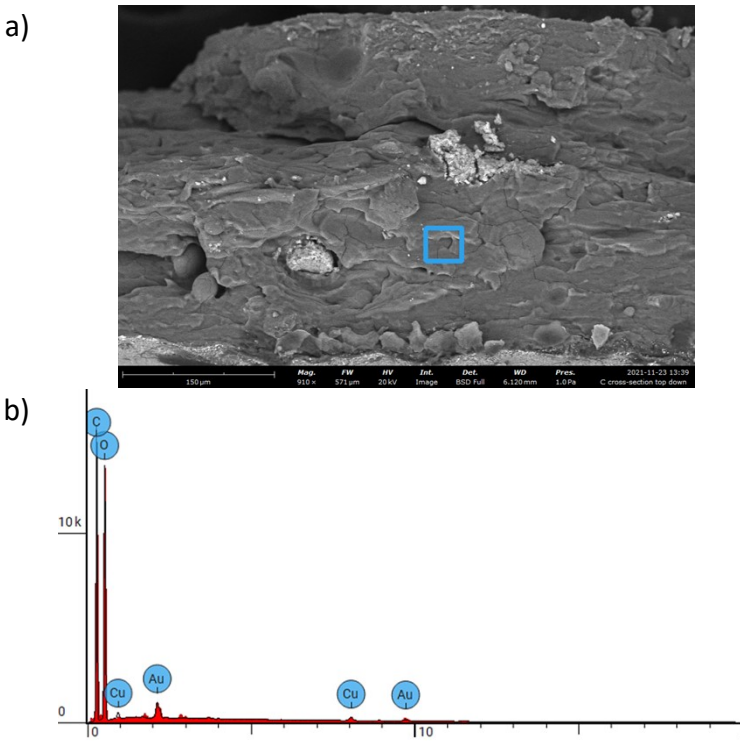

Figure S16. (a) Example of SEM image at 910× magnification of **2**-5%@$[PS]_n$ biopolymeric film with (b) EDS analysis of elemental composition (162 020 counts in 0:00:30 (5 378 c/s). Blue square in (a) shows an area deficient in Cu compound **2** (used for running EDS). The presence of Au in (b) is due to gold SEM coating.

Water Absorption by Biopolymers. In order to investigate water absorption by the obtained samples, the biopolymeric films (∅ = 0,9 cm) were submerged in water (10 mL; 36 °C), and their mass was determined after 4 and 24 h.

$$Wup\ (\%) = \frac{W_f - W_i}{W_i} \times 100$$

Table S2. Water absorption determination through mass weighing for $[PS]_n$ and $[PS\text{-}MCC]_n$ biopolymer films.

Sample	W_i (mg)[a]	W_f (mg)[b]		W_{up} (%)[c]	
	0 h	4 h	24 h	4 h	24 h
1@$[PS]_n$	16.7	24.6	24.2	32.1	31.0
1@$[PS\text{-}MCC]_n$	31.1	51.2	52.2	39.3	40.4
2@$[PS]_n$	20.8	29.7	28.9	30.0	28.0
3@$[PS]_n$	16.3	21.3	20.6	23.5	20.9
CuO@$[PS]_n$	12.2	22.2	22.0	45.0	44.5
CuO@$[PS\text{-}MCC]_n$	21.9	33.1	29.9	33.8	26.8

[a]Starting weight. [b]Weight after 4 and 24 h. [c]Water uptake weight percentage after 4 and 24 h.

Table S3. Copper release from degradable **1**@$[PS]_n$, **1**@$[PS\text{-}MCC]_n$, **2**@$[PS]_n$, **3**@$[PS]_n$, CuO@$[PS]_n$, and CuO@$[PS\text{-}MCC]_n$ samples after 4 and 24 h in aqueous Phosphate Buffered Saline solution.

Sample	Cu^{2+} release (mg/L)		Cu^{2+} release (% of all Cu in the sample)
	4 h	24 h	24 h
1@$[PS]_n$	0.35	0.38	27.5
1@$[PS\text{-}MCC]_n$	0.24	0.39	29.7
2@$[PS]_n$	0.10	0.32	15.4
3@$[PS]_n$	0.31	0.32	18.8
CuO@$[PS]_n$	0.45	0.47	6.4
CuO@$[PS\text{-}MCC]_n$	0.18	0.27	3.5

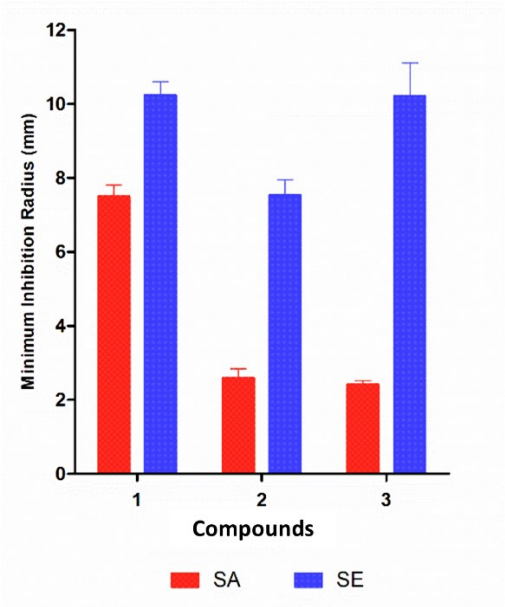

Figure S17. Nonnormalized antibacterial activity of **1**, **2**, and **3** against *S. aureus* (SA) ATCC 25923 and *S. epidermidis* (SE) RP62A (minimum inhibition radius (mean ± SD)).

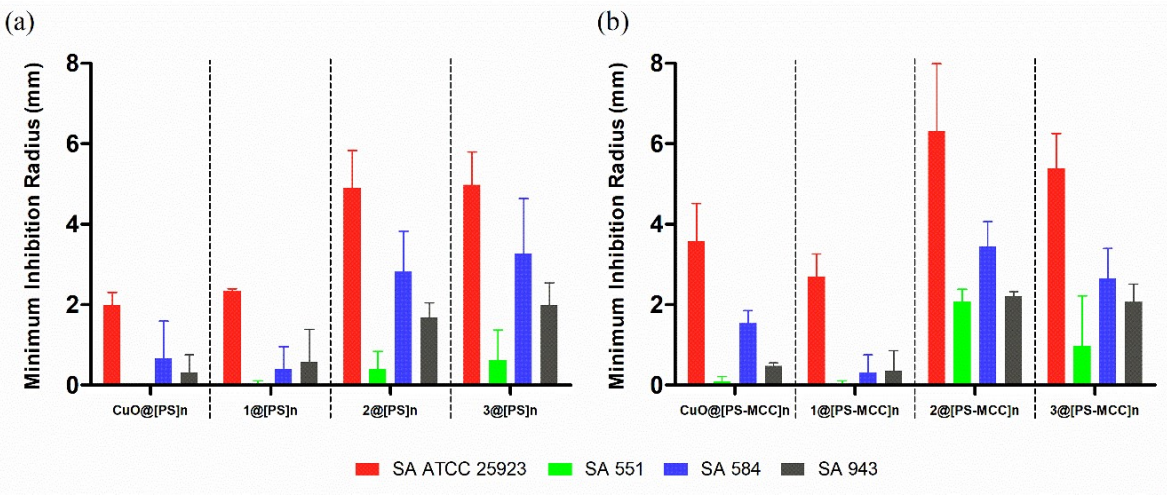

Figure S18. Nonnormalized antibacterial activity of $[PS]_n$ (a) and $[PS\text{-}MCC]_n$ (b) films doped with 5% of CuO (CuO@$[PS]_n$ and CuO@[PS-MCC]n), **1** (**1**@$[PS]_n$ and **1**@$[PS\text{-}MCC]_n$), **2** (**2**@$[PS]_n$ and **2**@$[PS\text{-}MCC]_n$), and **3** (**3**@$[PS]_n$ and **3**@$[PS\text{-}MCC]_n$) against four strains of *S. aureus* (SA), namely one reference strain (ATCC 25923) and three clinical isolates (551, 584, and 943).

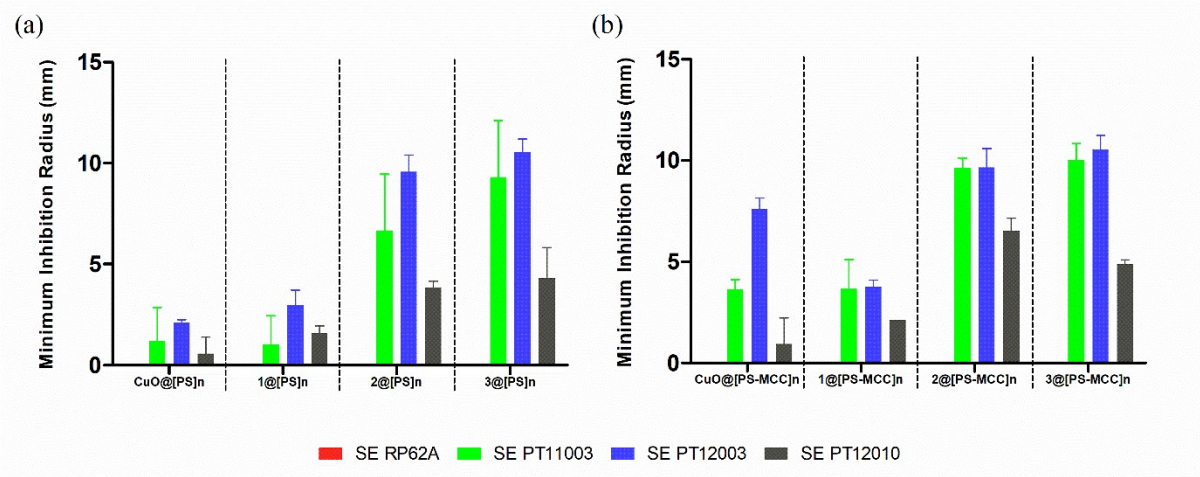

Figure S19. Nonnormalized antibacterial activity of $[PS]_n$ (a) and $[PS\text{-}MCC]_n$ (b) films doped with 5% of CuO ($CuO@[PS]_n$ and $CuO@[PS\text{-}MCC]_n$), **1** (**1**$@[PS]_n$ and **1**$@[PS\text{-}MCC]_n$), **2** (**2**@[PS]n and **2**$@[PS\text{-}MCC]_n$), and **3** (**3**$@[PS]_n$ and **3**$@[PS\text{-}MCC]_n$) against four strains of *S. epidermidis* (SE), namely one reference strain (RP62A) and three clinical isolates (PT11003, PT12003, and PT12010).

Table S4. Relevant Cu-based coordination complexes/polymers/MOFs and their antibacterial applications.

#	Formula	Cu environment	nD	Ligand	Type of bacteria	Antibacterial activity	Reference
1	$[Cu(4\text{-}OHNA)(bipy)H_2O](NO_3)$	Cu-O Cu-N	0D	4-hydroxynicotinic acid 2,2′- bipyridine	*B. subtilis* *S. aureus* *E. coli*	more active compare to free ligands	Srivastava *et al.*, 2020 [S4]
2	$[Cu(4\text{-}OHNA)(5,5'\text{-}Me_2bipy)(ONO_2)](H_2O)$	Cu-O Cu-N	0D	4-hydroxynicotinic acid 5,5′-dimethyl-2,2′-bipyridine			
3	$[Cu(4\text{-}OHNA)(phen)(H_2O)](NO_3)$	Cu-O Cu-N	0D	4-hydroxynicotinic acid 1,10-phenanthroline			
4	$[Cu(4\text{-}OHNA)(dmp)(ONO_2)](H_2O)$	Cu-O Cu-N	0D	4-hydroxynicotinic acid and 2,9-dimethyl-1,10-phenanthroline			
5	$[Cu(L)(bipy)]BF_4{\cdot}0.5H_2O$	Cu-O Cu-N	0D	4-(diethylamino)−2-hydroxybenzaldehyde 2,2′- bipyridine	*E. coli* *P. hauseri* *P. aeruginosa* *S. entérica* *S. aureus, B. subtilis* *K. rhizophila* *C. sporogenes* *A. brasiliensis* *S. cerevisiae* *C. albicans*	interference with normal cell processes	Dimitrijević *et al.*, 2020 [S5]
6	$[Cu_2(L)_2(phen)_2](BF_4)_2$	Cu-O Cu-N	0D	4-(diethylamino)−2-hydroxybenzaldehyde 1,10-phenanthroline			
7	$[Cu(CF_3SO_3)(H_2O)(pz)_4]CF_3SO_3$	Cu-O Cu-N	0D	pyrazine	*P. aeruginosa,* *S. aureus*	antimicrobial and antiproliferative activity	Glišić *et al.*, 2020 [S6]
8	$[Cu(NO_3)_2(H_2O)_2(qz)_2]$	Cu-O Cu-N	0D	quinazoline			
9	$[Cu(NO_3)_2(OH)_2(H_2O)_2(qz)_2]$	Cu-O Cu-N	0D	quinazoline			
10	$[Cu(NO_3)_2(H_2O)_2(pm)_2]_n$	Cu-O Cu-N	1D	pyrimidine			
11	$[CuCl_2(DEEI)]$	Cu-N Cu-Cl	0D	2-[2-[2-[2-(1,3-dioxoisoindol-2-yl)ethylamino]ethylamino]ethyl]isoindole-1,3-dione	*S. enterica,* *E. faecalis* *S. pneumoniae*	inhibitory action against biofilm formation	Arif *et al.*, 2020 [S7]
12	$[Cu(tmen)(succ)]_n{\cdot}4nH_2O$	Cu-O Cu-N	1D	succinate dianion and *N,N,N′,N′*-tetramethylethylenediamine	*B. spizizenii*, *E. coli*, *K. pneumonia*, *S. aureus*	significant antibacterial activity against Escherichia coli	Batool *et al.*, 2020 [S8]
13	$[\{Cu(muco)(bpa)(2H_2O)\}{\cdot}2H_2O]_n$	Cu-O Cu-N	3D	1,2-bis(4-pyridyl)ethane and *trans*-muconate dianion and *trans*-muconate dianion	*S. aureus*	inhibitory action against biofilm formation	Fu *et al.*, 2022 [S9]
14	$[\{Cu(muco)(4bpdp)\}{\cdot}2DMF{\cdot}H_2O]_n$	Cu-O Cu-N	3D	1,4-bis(4-pyridyl)-2,3-diaza-1,3-butadiene			
15	$H_3[(Cu_4Cl)_3(BTTri)_8\text{-}(DMF)_{12}]{\cdot}7DMF{\cdot}76H_2O$ (1-DMF)[a]	Cu-N Cu-Cl	3D	1,3,5-tris(1H-1,2,3-triazol-5-yl)benzene)	*P. aeruginosa*	biofilm inhibitor	Neufeld *et al.*, 2017 [S10-11], Demessence et al., 2009 [S12], McDonald et al. 2011 [S13]

[a] This was also supported on Chitosan

Supporting References

[S1] M. Kačuráková, M. Mathlouthi, FTIR and laser-Raman spectra of oligosaccharides in water: characterization of the glycosidic bond. *Carbohydr. Res.*, 1996, **284**, 145.

[S2] R. Kizil, J. Irudayaraj, K. Seetharaman, Characterization of irradiated starches by using FT-Raman and FTIR spectroscopy. *J. Agric. Food Chem.*, 2002, **50**, 3912.

[S3] J. J. Cael, K. H. Gardner, J. L. Koenig, J. Blackwell, Infrared and Raman spectroscopy of carbohydrates. Paper V. Normal coordinate analysis of cellulose. *J. Chem. Phys.*, 1975, **62**, 1145.

[S4] A.K. Srivastava, S.K. Singh, A. Srivastava, Spectral, biological antimicrobial activity (in vitro) and effect of solvents on the electrochemical behavior of four newly synthesized copper(II) complexes with 4-

hydroxynicotinic acid containing 2,2'-bipyridine/5,5'-Me2-bipy/1,10-phenanthroline/DMP, Chemical Data Collections, 2020, **26**, 100357.

[S5] T. Dimitrijević, I.Novaković, D. Radanović, S.B. Novaković, M.V. Rodić, K. Anđelković, M. Šumar-Ristović, Synthesis, spectral and structural characterization and biological activity of Cu(II) complexes with 4-(diethylamino)salicylaldehyde and α-diimines, *Journal of Coordination Chemistry*, 2020, **73**, 702.

[S6] B. Đ. Glišić, I. Aleksic, P. Comba, H. Wadepohl, T. Ilic-Tomic, J. Nikodinovic-Runic and M. I. Djuran, Copper(II) complexes with aromatic nitrogen-containing heterocycles as effective inhibitors of quorum sensing activity in Pseudomonas aeruginosa. *RSC Adv.*, 2016, **6**, 86695.

[S7] R. Arif; P.S. Nayab, I.A. Ansari, M. Shahid, M. Irfan, S. Alam, M. Abid, Synthesis, Molecular Docking and DNA Binding Studies of Phthalimide-Based Copper(II) Complex: In Vitro Antibacterial, Hemolytic and Antioxidant Assessment. *J. Mol. Struct.*, 2018, **1160**, 142.

[S8] S.S. Batool, S.R. Gilani, S.S. Zainab, M.N. Tahir, W.T.A. Harrison, M.Salman Haider, Q. Syed, S. Mazhar, M. Shoaib, Synthesis, crystal structure, thermal studies and antimicrobial activity of a new chelate complex of copper(II) succinate with N,N,N',N'-tetramethylethylenediamine, *Journal of Coordinations Chemistry*, 2020, **73**(12), 1778.

[S9] D. Fu, S. Yang, J. Lu, H. Lian, K. Qin, Two Cu(II) Coordination Polymers: Treatment Activity on Spine Surgery Incision Infection by Inhibiting the Staphylococcus aureus Biofilm Formation, *Journal of Cluster Science*, 2022, **33**, 529.

[S10] H.N. Rubin, B.H. Neufeld, M.M. Reynolds, Surface-Anchored Metal-Organic Framework-Cotton Material for Tunable Antibacterial Copper Delivery, *ACS Applied Materials and Interfaces*, 2018, **10**, 15189.

[S11] B.H. Neufeld, M.J. Neufeld, A. Lutzke, S.M. Schweickart, M.M. Reynolds, Metal–Organic Framework Material Inhibits Biofilm Formation of Pseudomonas aeruginosa, *Advanced Functional Materials*, 2017, **27**, 1702255.

[S12] A. Demessence, D.M. D'Alessandro, M.L. Foo, J.R. Long, Strong CO_2 binding in a water-stable, triazolate-bridged metal-organic framework functionalized with ethylenediamine, *J Am Chem Soc.*, 2009, **131**, 8784–8786.

[S13] T.M. McDonald, D.M. D'Alessandro, R. Krishna, J.R. Long, Enhanced carbon dioxide capture upon incorporation of N,N'- dimethylethylenediamine in the metal-organic framework CuBTTri, Chemical Science, 2011, **2**, 2022.